IEEE Access
Multidisciplinary ⋮ Rapid Review ⋮ Open Access Journal

Received 18 October 2023, accepted 6 November 2023, date of publication 8 November 2023,
date of current version 14 November 2023.

Digital Object Identifier 10.1109/ACCESS.2023.3331222

RESEARCH ARTICLE

AlGaN/GaN Distributed Schottky Barrier Single-Pole Single-Throw Millimeter-Wave Switches

PAWEŁ BAJURKO[1,2], (Member, IEEE), JAKUB SOBOLEWSKI[1,2], (Member, IEEE), YEVHEN YASHCHYSHYN[1,2], (Senior Member, IEEE), PAVLO SAI[2], SERGEY L. RUMYANTSEV[2], TEODOR NARYTNYK[2], AND GRZEGORZ CYWIŃSKI[2]

[1]Institute of Radioelectronics and Multimedia Technology, Warsaw University of Technology, 00-665 Warsaw, Poland
[2]CENTERA Laboratories, Institute of High Pressure Physics PAS, 01-142 Warsaw, Poland

Corresponding author: Paweł Bajurko (pawel.bajurko@pw.edu.pl)

This work was supported in part by the CENTERA Laboratories in the frame of the International Research Agendas Program for the Foundation for Polish Sciences co-funded by the European Union under the European Regional Development Fund under Grant MAB/2018/9; in part by the National Science Centre, Poland, under Grant 2016/22/E/ST7/00526 and Grant 2019/35/N/ST7/00203; and in part by the IMAGE Project funded by the European Union's Horizon2020 Research and Innovation Program under the Marie Skłodowska-Curie Grant under Agreement 778156.

ABSTRACT This paper presents two designs of millimeter-wave single-pole single-throw switches based on AlGaN/GaN heterostructure. The switches are based on two approaches to the travelling wave concept with Schottky barrier shunt elements integrated into a coplanar waveguide. The first design utilizes a two-stage artificial transmission line topology with distributed shunt elements in Schottky diode configuration. The second one employs a single electrically large shunt element configured as a high electron mobility transistor. Both arrangements allow the switches to achieve very high operational bandwidth, exceeding 100 GHz, without the requirement for very high lithography resolution. Examined switches were fabricated in a 2-μm GaN-on-SiC process. Measurement results demonstrate upper operating frequencies exceeding 114.5 GHz starting from 14 GHz or even DC, depending on the design. The W band on-off ratio over 17 dB and 21 dB is achieved by the first and second construction, respectively. Measurements of transient parameters show that high switching speed can also be achieved (rise/fall time as low as $\leq$17 ns for the first construction).

INDEX TERMS Millimeter-wave, SPST switch, RF switch, AlGaN/GaN, Schottky barrier, distributed shunt.

I. INTRODUCTION

The high-electron-mobility transistor (HEMT) developed on a GaN basis demonstrates exceptional capabilities, combining high voltage, high power, high speed, and high-temperature operation [1], [2], [3]. Furthermore, GaN-on-Si technology, which offers the potential for significant production cost reduction and is better suited for high-volume manufacturing, has garnered considerable attention [4]. Nevertheless, the challenge lies in the substantial mismatch in lattice constant and thermal expansion between Si substrates and GaN, making it more difficult to achieve high-quality GaN growth on Si substrates. This obstacle often necessitates the use of thicker or more complex buffer layer structures [5], [6]. When SiC substrates are used, the lattice constant and thermal expansion coefficient mismatch are minimized. Consequently, the quality of GaN epitaxy grown on SiC is improved. Additionally, SiC substrates exhibit excellent thermal conductivity, efficiently dissipating the heat generated by GaN HEMTs during high-frequency operations, thereby enhancing overall reliability [7].

High flexibility and dynamic reconfigurability are important goals for the development of modern radio frequency (RF) systems. One of the key components enabling such features are RF switches. As the millimeter-waves (mm-waves) continue to find an increasing number of applications in communication, sensing, imaging, testing, and instrumentation systems, efficient devices operating in this

The associate editor coordinating the review of this manuscript and approving it for publication was Rocco Giofrè.

region are necessary. Time-modulated antenna arrays are one of the growing applications where optimizing switch parameters is of paramount importance to ensure high performance [8], [9]. GaN semiconductors offer good high frequency characteristics and can be a prospective solution for RF applications. However, development and optimization of building blocks like GaN switches is required to achieve satisfactory performance of on-chip integrated systems [10], [11].

A single-pole single-throw (SPST) switch is a basic building block for signal control in RF systems as well as a part of multiple-throw switching circuits. In the literature, there are many examples of switch designs applying one of the two main topologies: shunt or series [12]. The most frequently used is shunt topology, where a switching element, typically a transistor or a diode, is used to create a short circuit in the transmission line. The shunt switching element is generally better suited for wide bandwidth operation than series one because when used directly in the transmission line, its parasitic capacitance is connected in parallel to the naturally present distributed capacitance of the transmission line and does not significantly harm the operation of the line. In contrast, the parasitic capacitance of the series element resides in the line discontinuity, where its presence has solely undesirable effects by reducing the isolation at high frequencies [13], [14], [15]. The shunt and series elements can also be combined in series-shunt topology to isolate inactive paths in multiple-throw switches without using quarter-wave transformers [16], [17].

A notable group of switch designs is based on various types of resonant circuits. These constructions are inherently narrowband, however, they allow to achieve very low insertion loss and high isolation [16], [18], [19]. Nonetheless, wider bandwidth devices using high order resonator circuits can also be found [20], [21].

In order to increase the bandwidth travelling wave switch concept was proposed [22], [23]. In this type of construction, instead of a single shunt element, multiple stages of shunt elements separated by transmission line sections are used. Such a design constructively exploits parasitic capacitances of switching elements to create an artificial transmission line. In the on-state, the line exhibits low losses in very wide bandwidth. Isolation in the off-state can also be significantly improved. To illustrate the benefits of travelling wave switch design, an example shown in Fig. 1 is used. It compares single element shunt SPST switch against three stage travelling wave construction (Fig. 1a). For this comparison, simplified models of shunt transistors are used. In the on-state, the transistors are represented by their parasitic capacitances (Fig. 1b), while in the off-state – by their channel resistances (Fig. 1c). Travelling wave switch presents significantly improved characteristics in terms of insertion loss, reflection coefficient, and isolation (Fig. 1d), while the overall gate width of transistors used in both models remains the same. It should be noted that very limited number of shunt elements is required to create a broadband artificial transmission line,

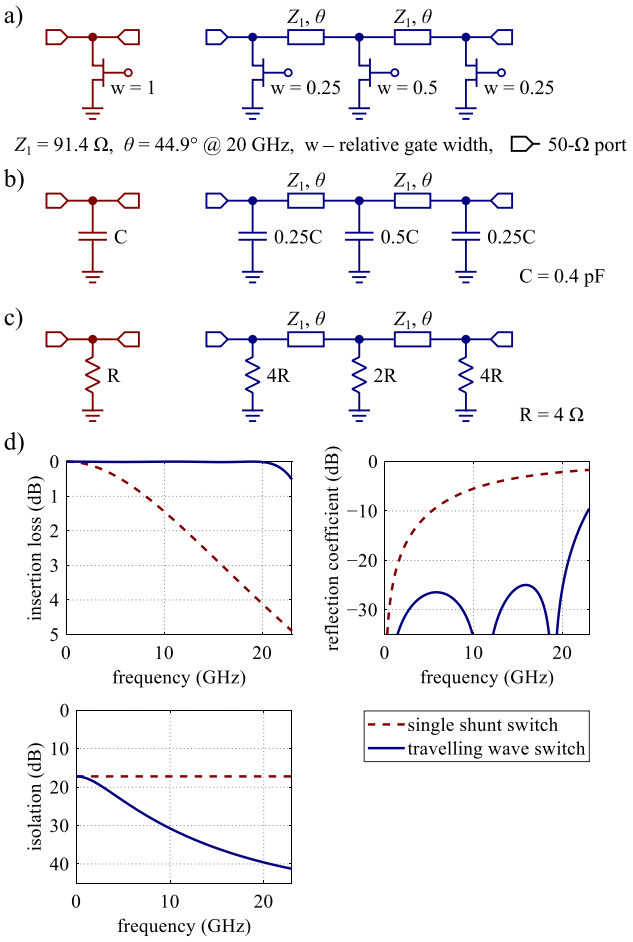

FIGURE 1. Example comparison between single shunt (chestnut color) and travelling wave (navy blue color) SPST switches. a) Schematic diagrams of the switches. b) Equivalent circuits in on-state. c) Equivalent circuits in off-state. d) Simulation results.

even 2 or 3 as shown in the example. Therefore, such a construction can be relatively compact. Published implementations of travelling wave switches can be found in [10], [22], [23], and [24].

If a shunt transistor is sufficiently small, it can be regarded as a lumped element. At the mm-waves range this can be achieved with contemporary high-resolution semiconductor processing (100 nm or less). In travelling wave concept, these lumped elements are used to create an electrically large distributed structure. However, the similar effect can also be achieved with a much larger size of the shunt elements, which constitute distributed parts by themselves. This can significantly reduce the requirement for the manufacturing process resolution. Also, in this application, the transistors may operate at frequencies above their transition frequency, as they are not used as active components.

This paper presents two designs of AlGaN/GaN mm-wave SPST distributed shunt switches integrated with a coplanar waveguide (CPW). Both designs employ the travelling wave switch concept. The first uses two-stage construction with Schottky diode shunt elements, while the second utilizes

single electrically large transistor shunt element. None of them requires a high-resolution fabrication process as the smallest details of both layouts are not finer than 2 μm. The designed switches were fabricated and characterized in the frequency range up to 114.5 GHz. Also, the transient characteristics were measured. The paper includes an analysis of the impact of different design features on the switches performance.

II. SWITCHES DESIGNS

Schottky barrier switching elements used in both proposed designs are distributed, i.e., their dimensions are comparable to the wavelength as opposed to lumped elements typically used in RF switches. The switching elements are embedded in CPW and arranged in the shunt configuration. In the off-state, they create a short-circuit in the waveguide, therefore the proposed devices operate as reflective switches.

The switches are fabricated based on the AlGaN/GaN semiconductor structure typical for HEMT for high-frequency applications [2], [25]. AlGaN/GaN epitaxial heterostructures were grown by Metalorganic Vapor Phase Epitaxy (MOVPE) on a silicon carbide substrate. MOVPE growth was initialized from a 38 nm thick AlN nucleation layer on a commercially available 500-μm-thick semi-insulating SiC substrate. Then, a 2.3 μm high-resistivity (HR) GaN buffer was applied, followed by a 0.7 μm unintentionally doped (UID) GaN layer. The AlGaN barrier consisted of: 1.2 nm $Al_xGa_{1-x}N$ (x = 66%), 5 nm $Al_xGa_{1-x}N$ UID (x = 28%), 10 nm AlGaN:Si (n$\sim$1.5 $\times$ 10^{18} cm^{-3}), and a 2 nm UID AlGaN layer. The whole heterostructure was covered by a 2 nm GaN cap layer.

At the AlGaN/GaN heterointerface, the 2-dimensional electron gas (2DEG) is formed, which constitutes the channel in semiconductor devices. In proposed devices, 2DEG channel creates a shunt connection from the center line of the CPW to the ground. An electrode made of metal placed over the 2DEG forms Schottky junction, the polarization of which can be used to control the conductivity of the channel. When the junction is reverse biased, the 2DEG is depleted, resulting in increased resistivity of the shunt element (on-state of the switch). Without bias, the 2DEG resistivity is approximately 400 Ω/sq. When embedded in the CPW, such a component makes the waveguide section highly lossy (off-state of the switch).

A. SWITCH TYPE A

Switch type A shunt element operates in a lateral Schottky diode configuration [26] shown in Fig. 2. The 2DEG is a cathode of the diode, and metal Schottky electrode is an anode. The cathode is connected to the ground conductor of the CPW via ohmic contact. The ohmic contact was created by Ti/Al/Ni/Au layers deposition and rapid thermal annealing at 800°C for 60 s. The anode is connected to the center conductor of the CPW along the whole length of the shunt element and overlaps the 2DEG by 3 μm to create

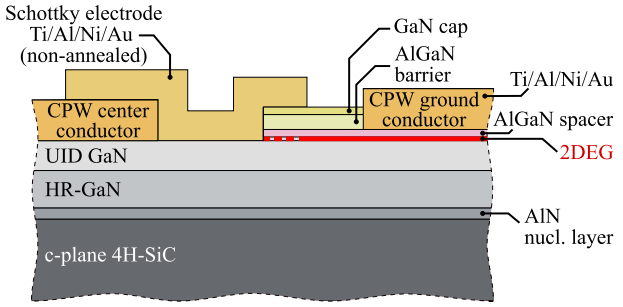

FIGURE 2. Cross-section diagram of the switch type A shunt element.

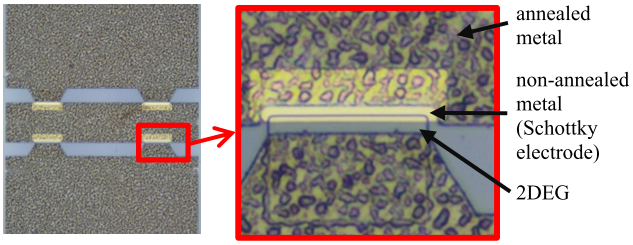

FIGURE 3. Fabricated structure of the switch type A [27].

lateral Schottky contact. The anode was created by Ni/Au metallization deposition without any following annealing. The diode configuration of the shunt element allows to apply a control voltage through the center conductor of the CPW together with the RF signal. In order to turn on the switch, the diode has to be reverse polarized, therefore the negative control voltage is required.

The switch type A uses double stage travelling wave construction with two 50 μm long shunt elements placed 175 μm apart, embedded in the coplanar waveguide (Fig. 3). This arrangement takes advantage of the artificial transmission line concept to achieve low insertion and return loss as well as high isolation of the switch at frequencies exceeding 100 GHz.

To analyze double stage construction and its advantages over single stage one, RF equivalent circuits of these variants were developed (Fig. 4). The single stage circuit (Fig. 4a) consists of two sections of CPW and a section of distributed shunt element between them. The CPW is represented by the conventional lumped-element transmission line model [28] and the shunt section by the modified lumped-element transmission line model shown in Fig. 4c and d, respectively. The additional conductance G_{2DEG} in the modified model is used to take into account the distributed conductivity of 2DEG in the shunt element.

In the double stage circuit (Fig. 4b), two shunt sections are used with a CPW section in between. The shunt section length in the single stage switch is two times larger than in the double-stage switch. Parameters of both transmission line models were established from test structures measurements, with the latter depending on the state of the switch. Their values are gathered in Table 1.

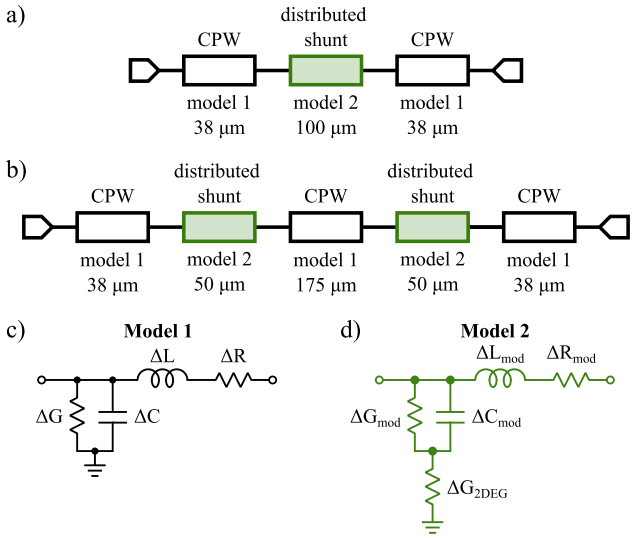

FIGURE 4. Model of a) single stage, b) double stage shunt switching device; c) Lumped-element transmission line model; d) Modified lumped-element transmission line model. Parameters of transmission line models are normalized per unit length.

TABLE 1. Parameter values for switch A transmission line models.

	Parameter	Value	
model 1	ΔR	20 + 0.419·f [GHz] kΩ/m	
	ΔL	408 nH/m	
	ΔG	0 S/m	
	ΔC	163 pF/m	
		on-state	off-state
model 2	ΔR_{mod}	20 + 0.419·f[GHz] kΩ/m	20 + 0.419·f[GHz] kΩ/m
	ΔL_{mod}	122 nH/m	345 nH/m
	ΔG_{mod}	0 S/m	0 S/m
	ΔC_{mod}	559 pF/m	16.3 nF/m
	ΔG_{2DEG}	∞	1.11 kS/m

Calculated transmission and reflection coefficients of the switch equivalent circuits are shown in Fig. 5a and b, respectively. Insertion loss in the on-state is similar for both switches, however, in the off-state the double stage switch exhibits superior isolation at mm-wave frequencies (Fig. 5a). On-state reflection coefficient characteristic of double stage switch shows expected return loss improvement at mm-wave frequencies compared to single stage construction (Fig. 5b).

It can be noticed that the isolation of modelled switches degrades significantly at very low frequencies (Fig. 5a). It is caused by the fact that in the off-state, the shunt element does not provide short-circuit at DC. The advantage of this solution is the possibility to provide DC control voltage via RF path.

B. SWITCH TYPE B

Switch type B also utilizes travelling wave switch concept, however instead of using the artificial transmission line, a single distributed shunt element is applied. This electrically large component acts as a continuous switchable transmission line section in contrast to the chain of discrete elements forming the artificial transmission line.

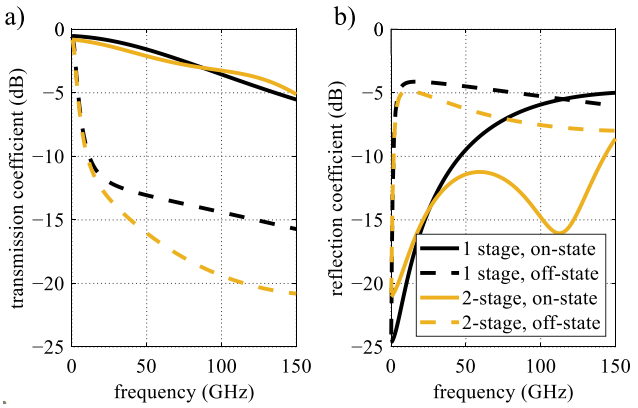

FIGURE 5. Calculated a) transmission, b) reflection characteristics of single and double stage shunt switch models from Fig. 4.

The semiconductor stack of the switch type B is the same as in type A. However, the transistor configuration is used instead of a diode (Fig. 6). In this configuration, the 2DEG channel extends from the ground to the center conductor of the CPW. Both conductors have ohmic contact to the 2DEG. Schottky electrodes are placed in the middle of the CPW gaps along the whole length of the shunt element and connected to a separate bias contact pad (Fig. 7). Such an arrangement of the electrodes forms a vertical Schottky contact to 2DEG channel. Transistor configuration requires negative control voltage on the Schottky electrode to deplete the 2DEG and, in consequence, turn on the switch.

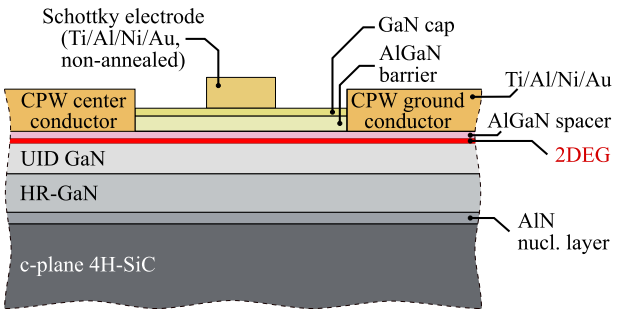

FIGURE 6. Cross-section diagram of the switch type B shunt element.

The gate length of the shunt transistor equals 2 μm with the channel length of 8 μm. Dimensions of the CPW are tailored to minimize characteristic impedance discontinuities between the shunt section and the rest of the CPW.

The RF equivalent circuit of switch B is shown in Fig. 8. The structure of the model is the same as the model shown in Fig. 4a, however, the length of the shunt element is increased to 300 μm. Parameters of the models given in Table 2 are adjusted to reflect the different geometry of the CPW and distributed shunt element.

Calculated transmission and reflection coefficients of the switch B equivalent circuit are shown in Fig. 9a and b, respectively. The most significant differences compared to switch A are greatly improved isolation and operation of

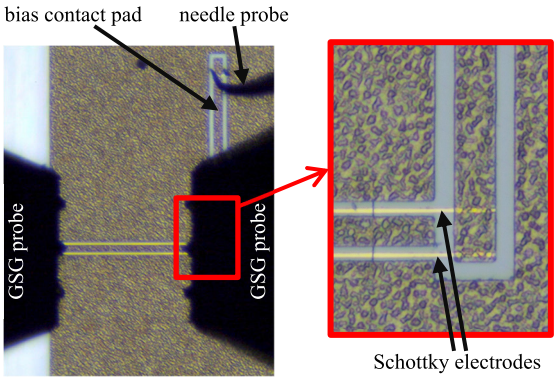

FIGURE 7. Fabricated structure of the switch type B [27].

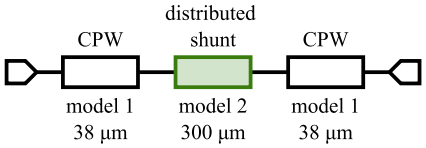

FIGURE 8. Model of the switch type B.

TABLE 2. Parameter values for switch B transmission line models.

	Parameter	Value	
model 1	ΔR	$79 + 0.33 \cdot f$ [GHz] kΩ/m	
	ΔL	453 nH/m	
	ΔG	0 S/m	
	ΔC	181 pF/m	
		on-state	**off-state**
model 2	ΔR_{mod}	$54.7 + 0.545 \cdot f$[GHz] kΩ/m	$53 + 1.1 \cdot f$[GHz] kΩ/m
	ΔL_{mod}	346 nH/m	1 nH/m
	ΔG_{mod}	0 S/m	354 S/m
	ΔC_{mod}	317 pF/m	1.27 nF/m
	ΔG_{2DEG}	1250 S/m	∞

the switch from DC. The insertion loss is higher, mainly due to narrower center conductor of the transmission lines. Despite that, the on-off ratio is notably higher compared to switch A. The advantage of the narrower center conductor is reduction of characteristic impedance changes along the length of the device. It allowed to maintain low on-state return loss in the wide bandwidth even though single stage design is employed. The simulation results allow to conclude that single distributed shunt element can provide wideband operation of the switch.

The main features of the proposed switches are gathered in Table 3.

III. MEASUREMENTS

A. MEASUREMENT SETUP

The manufactured switches were measured in two frequency ranges. For measurements in the lower range, from 10 MHz to 50 GHz, measurement setup A (Fig. 10a) was used with Agilent N5245A PNA-X vector network analyzer (VNA) connected to the device under test (DUT) using a 100 μm pitch Cascade Microtech Infinity GSG probes. The probes

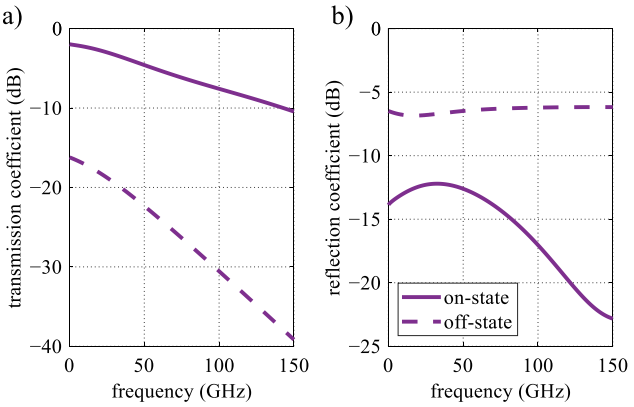

FIGURE 9. Calculated a) transmission, b) reflection characteristics of switch B model from Fig. 8.

TABLE 3. Comparison of the designs.

Switch type	A	B
Switch configuration	double shunt travelling wave	single electrically large shunt
Schottky contact configuration	lateral	vertical
Shunt device	diode	transistor
Shunt length	2×50 µm, 175 µm spacing	300 µm
CPW center conductor width	80 µm	14 µm
Control voltage connection	via RF port	via separate electrode
Control voltage polarization	negative	negative

were positioned using the Cascade Microtech EPS200MMW probe station. In the case of switch A, control voltage was applied to the center line of the CPW via GSG probes using external bias ports of the VNA. Switch B was controlled by the voltage applied to the bias contact pad via additional needle probe. The control voltage connections to the DUT are illustrated in Fig. 11.

For measurements in the higher range, from 70.5 GHz to 114.5 GHz, measurement setup B (Fig. 10b) was used. In this setup, the VNA was connected to a pair of VDI WR-10 waveguide frequency extenders with 100 μm pitch Cascade Microtech Infinity WR-10 waveguide GSG probes. Bias voltage for switch A was provided via bias ports on the probes. For the calibration and setting the measurement plane to the contact pads, the Cascade 101-190C and Cascade 138-357 standard impedance substrates were used at lower and higher frequency range, respectively.

B. RF CHARACTERISTICS

Measured transmission and reflection coefficient characteristics in both frequency ranges are presented in Fig. 12. The on-state transmission characteristics of both devices (Fig. 12a, solid lines) exhibit very broadband operation with

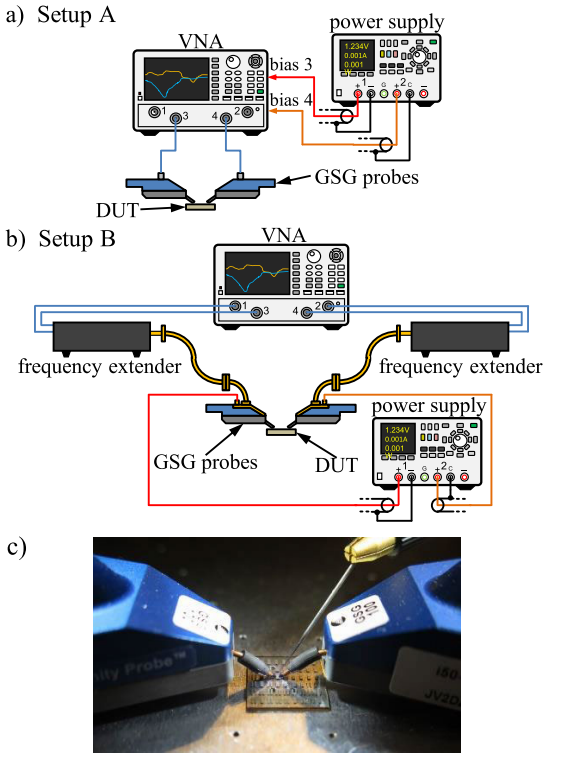

FIGURE 10. Schematic diagram of measurement setup: a) A for 10 MHz – 50 GHz, b) B for 70.5 – 114.5 GHz frequency range. c) Photo of the measurement setup A.

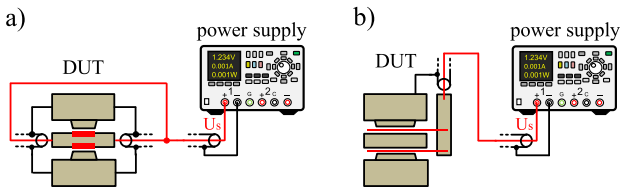

FIGURE 11. Schematic diagram of bias voltage supply for: a) switch A controlled through RF port, b) switch B controlled through external electrode.

insertion loss increasing slightly with frequency. However, switch A shows significantly lower insertion loss (under 3.5 dB in the whole measured frequency range).

The off-state transmission characteristics are shown in Fig. 12a with dashed lines. The isolation of both switches increases with frequency and above 100 GHz reaches 22 dB and 29 dB for switches A and B, respectively. Switch A exhibits a significant decrease of the isolation below 20 GHz, which is related to the construction of the shunt element (described in Section II-A). This restriction does not apply to switch B, which operates in the whole measurement frequency range, from DC to 114.5 GHz, with isolation above 16 dB.

Reflection coefficient characteristics in the off-state (Fig. 12b, dashed lines) show relatively high values for both switches as both are reflective RF switches. More important for the switch performance are the on-state reflection coefficient characteristics (Fig. 12b, solid lines). The one for switch A closely resembles the simulated characteristics

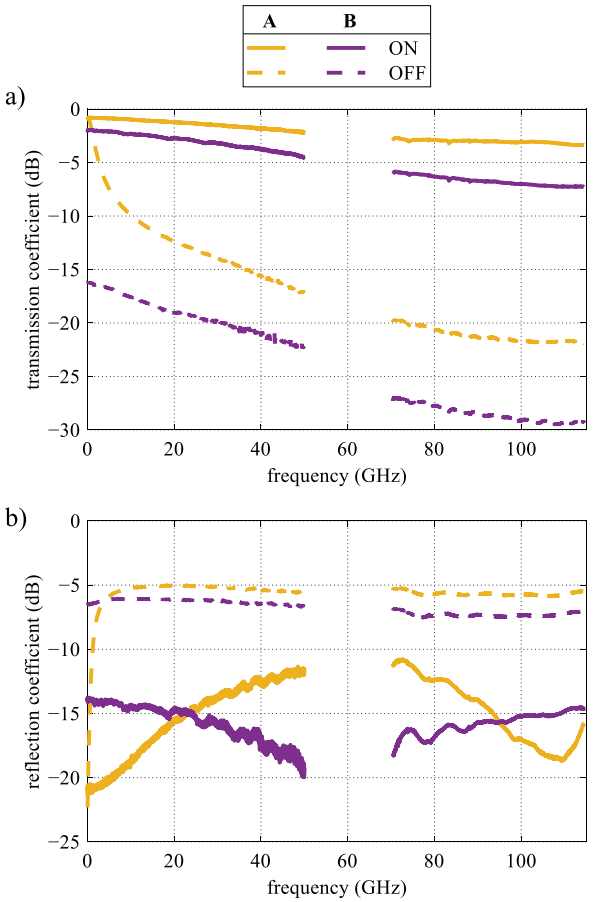

FIGURE 12. Measured transmission (a) and reflection (b) characteristics in off- (0 V) and on-state (−5 V).

shown in Fig. 5b, proving the validity of the artificial transmission line model incorporating distributed shunt elements. Switch B result (reflection coefficient below −14 dB in the whole measurement frequency range) shows that wideband matching can also be achieved with a single distributed electrically large shunt element corroborating findings from simulations (Fig. 9).

Although the measurement setups do not cover the 50–70.5 GHz frequency range, it can be seen that the trends observed in the lower and upper bands are consistent. Combined with the simulation results, it allows to assume that there should not be any notable deviations from these trends in the frequency gap. It should be also noted that although the upper measurement frequency limit was 114.5 GHz, the characteristics of the switches indicate that they can operate above the measurement bandwidth. It is especially the case for switch B, which exhibits relatively flat reflection coefficient characteristic at the highest measurement frequencies.

C. TRANSIENT CHARACTERISTICS

Transient characteristics of the switches were measured at a frequency of 38 GHz. Fig. 13a and 13c present turn-on transient characteristics normalized to the on-state

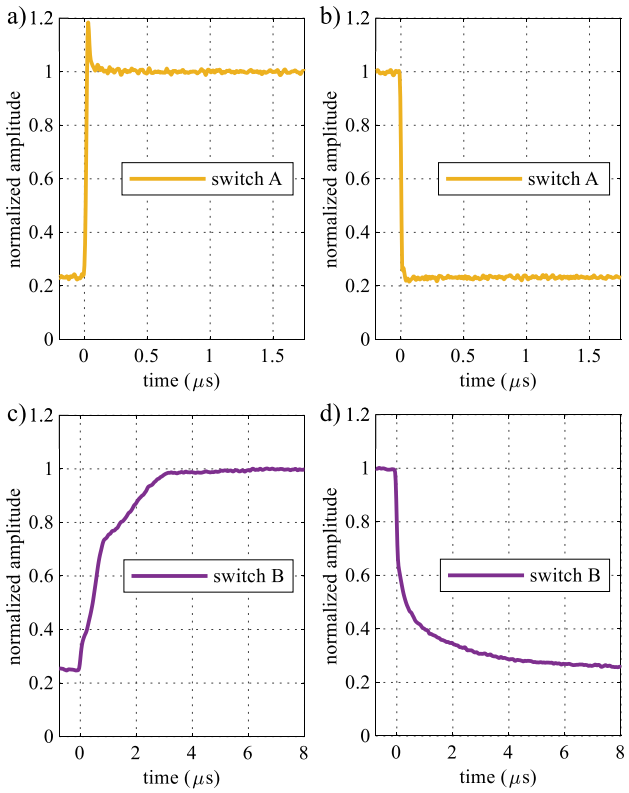

FIGURE 13. Switch-on (a, c) and switch-off (b, d) transient characteristics of output RF voltage envelope of the switches measured at 38 GHz. The waveforms are normalized to their own amplitude in steady on-state.

RF voltage level. Switch A exhibits a rise time not exceeding 17 ns, significantly shorter than switch B. In the turn-on process of switch B, at least two phases can be distinguished. The first phase has noticeably shorter time constant than the second. This behavior may result from metal layer defects locally decreasing the conductivity of the Schottky electrodes. Switch B comprises relatively long and narrow electrodes driven only from one side, which makes them susceptible to imperfections. When such a defect occurs, a part of the electrode can operate more slowly, resulting in a two-phase switching characteristic. It can also differently affect the electrodes on both sides of the CPW, leading to a similar effect.

Turn-off transient characteristics are shown in Fig. 13b and 13d. Switch A exhibits very short fall times, not exceeding 15 ns. Switch B exhibits excessively long fall time. As it is consistent with long rise time, the defects of the Schottky electrodes are the most likely cause of this behavior.

The measured switching times are gathered in Table 4. The times for switch A can not be strictly determined as they are reaching the resolution limits of the measurement equipment. Nevertheless, switch A can be considered high speed compared to commercially available mm-wave switches. In contrast, switch B operates at much lower speeds. However, this behavior may originate from accidental defects, as explained above. Therefore, the results for switch B are not conclusive with only one specimen of the switch examined. It should be noticed that defects causing observed inferior transient performance do not affect steady-state characteristics. This lends credence to the hypothesis that the defects relate to the conductivity of the control electrodes. Further investigation and tuning of manufacturing processes' parameters are required to improve the quality of the Schottky metal layer. Another possible solution to improve the transient characteristics of switch B can be a change in the Schottky electrodes design. For example, providing more than one connection to the bias contact pad could mitigate the influence of the defects.

TABLE 4. Measured switching times (between 10% and 90% of the RF voltage).

Switch type	A	B
Rise time	$\leq$ 17 ns	2375 ns
Fall time	$\leq$ 15 ns	5580 ns

IV. CONCLUSION

Two SPST switch designs based on the AlGaN/GaN semiconductor are presented. Both designs employ travelling wave concept with distributed shunt switching elements embedded in the transmission line. Switch A is a two-stage device constructed using artificial transmission line topology with distributed shunt elements in a diode configuration. Switch B is based on a single electrically large distributed shunt element in transistor configuration. Application of travelling wave concept allows to achieve wide bandwidth operation. Table 5 compares the proposed devices against other state-of-the-art mm-wave GaN switches. Both switches, A and B, exhibit significantly wider bandwidth than other compared devices. Particularly, switch B allows operation down to DC, which is a relatively rare feature of RF switches. Switch A also operates down to very low frequencies, however its on-off ratio decreases below 10 dB under 14 GHz due to the diode configuration of the switching element. Moreover, the measured characteristics indicate that the operational frequency range of the investigated switches can extend even beyond the upper measurement frequency limit.

The experimental evaluation shows that the proposed designs can achieve very low switching times (under 17 ns in case of switch A). However, examination of switch B indicates that large switching components are susceptible to manufacturing defects, which can significantly impact switching speed.

It should be noted that the presented designs based on the distributed shunt elements have very modest fabrication process resolution requirements, therefore they can be manufactured without the most sophisticated tools (e.g., a regular UV mask aligner machine can be used instead of deep/extreme UV or e-beam machine). It was shown that 2-μm resolution is sufficient to create switches operating over 100 GHz with satisfactory performance.

TABLE 5. State-of-the-art mm-wave GaN HEMT SPST switches.

Switch type	Frequency (GHz)	IL (dB)	Isolation (dB)	Ref
SPST, two stage 100-nm GaN-on-Si	26.2–36	1.1–1.6	43–47	[29]
SPST, four stage 100-nm GaN-on-Si	24.2–36.3	1.75–2.25	>56	[29]
SPST four stage 250-nm GaN	2.7–36.3	0.64–1.64	16.5–28	[24]
SPST, resonator, 100-nm GaN-on-Si	11–40.5	0.55–1	27–37	[21]
SPST 100-nm GaN-on-Si	20–44.8	0.62–1.1	>34	[30]
SPST 40-nm GaN on SiC	60–110	0.9–1.4	8–10	[31]
SPST 40-nm GaN on SiC	75–110	0.9–3.5	25–30	[32]
SPST type A, two stage 2-µm GaN on SiC	14–114.5+ (W band 75–110)	1.1–3.4 (2.8–3.3)	11.1–21.9 (20.2–21.8)	this work
SPST type B 2-µm GaN on SiC	DC–114.5+ (W band 75–110)	1.9–7.2 (6.0–7.2)	16.2–29.5 (27.3–29.5)	this work

ACKNOWLEDGMENT

Co-funded by the European Union (ERC "TERAPLASM", project number: 101053716). Views and opinions expressed are however those of the authors only and do not necessarily reflect those of the European Union or the European Research Council. Neither the European Union nor the granting authority can be held responsible for them.

REFERENCES

[1] U. K. Mishra, S. Likun, T. E. Kazior, and Y.-F. Wu, "GaN-based RF power devices and amplifiers," *Proc. IEEE*, vol. 96, no. 2, pp. 287–305, Feb. 2008, doi: 10.1109/JPROC.2007.911060.

[2] R. S. Pengelly, S. M. Wood, J. W. Milligan, S. T. Sheppard, and W. L. Pribble, "A review of GaN on SiC high electron-mobility power transistors and MMICs," *IEEE Trans. Microw. Theory Techn.*, vol. 60, no. 6, pp. 1764–1783, Jun. 2012, doi: 10.1109/TMTT.2012.2187535.

[3] U. K. Mishra, P. Parikh, and Y.-F. Wu, "AlGaN/GaN HEMTs—An overview of device operation and applications," *Proc. IEEE*, vol. 90, no. 6, pp. 1022–1031, Jun. 2002, doi: 10.1109/JPROC.2002.1021567.

[4] H. W. Then, M. Radosavljevic, N. Desai, R. Ehlert, V. Hadagali, K. Jun, P. Koirala, N. Minutillo, R. Kotlyar, A. Oni, M. Qayyum, J. Rode, J. Sandford, T. Talukdar, N. Thomas, H. Vora, P. Wallace, M. Weiss, X. Weng, and P. Fischer, "Advances in research on 300 mm gallium nitride-on-Si(111) NMOS transistor and silicon CMOS integration," in *IEDM Tech. Dig.*, Dec. 2020, pp. 27.3.1–27.3.4, doi: 10.1109/IEDM13553.2020.9371977.

[5] S. Nakamura, "GaN growth using GaN buffer layer," *Jpn. J. Appl. Phys.*, vol. 30, no. 10, Oct. 1991, Art. no. L1705, doi: 10.1143/JJAP.30.L1705.

[6] S. L. Selvaraj, A. Watanabe, A. Wakejima, and T. Egawa, "1.4-kV breakdown voltage for AlGaN/GaN high-electron-mobility transistors on silicon substrate," *IEEE Electron Device Lett.*, vol. 33, no. 10, pp. 1375–1377, Oct. 2012, doi: 10.1109/LED.2012.2207367.

[7] C. F. Campbell, A. Balistreri, M.-Y. Kao, D. C. Dumka, and J. Hitt, "GaN takes the lead," *IEEE Microw. Mag.*, vol. 13, no. 6, pp. 44–53, Sep. 2012, doi: 10.1109/MMM.2012.2205829.

[8] G. Bogdan, K. Godziszewski, Y. Yashchyshyn, C. H. Kim, and S.-B. Hyun, "Time-modulated antenna array for real-time adaptation in wideband wireless systems—Part I: Design and characterization," *IEEE Trans. Antennas Propag.*, vol. 68, no. 10, pp. 6964–6972, Oct. 2020, doi: 10.1109/TAP.2019.2902755.

[9] G. Bogdan, P. Bajurko, and Y. Yashchyshyn, "Time-modulated antenna array with dual-circular polarization," *IEEE Antennas Wireless Propag. Lett.*, vol. 19, no. 11, pp. 1872–1875, Nov. 2020, doi: 10.1109/LAWP.2020.2999643.

[10] T. Kim, H. Im, S.-H. Lee, K.-J. Kim, and C. Park, "Highly linear K-/Ka-band SPDT switch based on traveling-wave concept in a 150-nm GaN pHEMT process," *IEEE Microw. Wireless Compon. Lett.*, vol. 32, no. 8, pp. 987–990, Aug. 2022, doi: 10.1109/LMWC.2022.3161498.

[11] A. Biondi, F. Scappaviva, L. Cariani, F. Vitulli, F. Coromina, and F. Deborgies, "A Ka-band GaN 2 × 4 MMIC switch for compact and scalable switch matrices," in *Proc. 17th Eur. Microw. Integr. Circuits Conf. (EuMIC)*, Sep. 2022, pp. 25–28, doi: 10.23919/EuMIC54520.2022.9923543.

[12] J. Sobolewski and Y. Yashchyshyn, "State of the art sub-terahertz switching solutions," *IEEE Access*, vol. 10, pp. 12983–12999, 2022, doi: 10.1109/ACCESS.2022.3147019.

[13] Y. Yashchyshyn, P. Bajurko, J. Sobolewski, P. Sai, A. Przewłoka, A. Krajewska, P. Prystawko, M. Dub, W. Knap, S. Rumyantsev, and G. Cywiński, "Graphene/AlGaN/GaN RF switch," *Micromachines*, vol. 12, no. 11, p. 1343, Oct. 2021, doi: 10.3390/mi12111343.

[14] A. Singh and M. K. Mandal, "Parasitic compensation and hence isolation improvement of PIN diode-based switches," *IEEE Trans. Circuits Syst. II, Exp. Briefs*, vol. 68, no. 1, pp. 97–101, Jan. 2021, doi: 10.1109/TCSII.2020.3000587.

[15] F. Drillet, J. Loraine, H. Saleh, I. Lahbib, B. Grandchamp, L. Iogna-Prat, I. Lahbib, O. Sow, A. Kumar, and G. U'Ren, "RF small and large signal characterization of a 3D integrated GaN/RF-SOI SPST switch," *Int. J. Microw. Wireless Technol.*, vol. 13, no. 6, pp. 517–522, Jul. 2021, doi: 10.1017/s1759078721000076.

[16] T. Kim, H. D. Lee, B. Park, S. Jang, S. Kong, and C. Park, "Design of a K-band high-linearity asymmetric SPDT CMOS switch using a stacked transistor," *IEEE Microw. Wireless Compon. Lett.*, vol. 32, no. 12, pp. 1443–1446, Dec. 2022, doi: 10.1109/LMWC.2022.3192440.

[17] M. Di, Z. Pan, F. Zhang, C. Li, H. Wang, and A. Wang, "A study of ESD-mmWave-switch co-design of 28 GHz distributed travelling wave switch in 22 nm FDSOI for 5G systems," *IEEE J. Electron Devices Soc.*, vol. 9, pp. 1290–1296, 2021, doi: 10.1109/JEDS.2021.3131109.

[18] Y. Ahmed, A. Ezz, and M. El-Nozahi, "A 24–47-GHz resonant multi-band T/R switch," *IEEE Microw. Wireless Compon. Lett.*, vol. 31, no. 5, pp. 493–496, May 2021, doi: 10.1109/LMWC.2021.3067143.

[19] H. Takasu, F. Sasaki, H. Kawasaki, H. Tokuda, and S. Kamihashi, "W-band SPST transistor switches," *IEEE Microw. Guided Wave Lett.*, vol. 6, no. 9, pp. 315–316, Sep. 1996, doi: 10.1109/75.535830.

[20] D. Lu, J. Liu, and M. Yu, "Highly selective bandpass switch block with applications of MMIC SPDT switch and switched filter bank," *IEEE Solid-State Circuits Lett.*, vol. 5, pp. 190–193, 2022, doi: 10.1109/LSSC.2022.3194410.

[21] G. Shen, H. Zhu, Q. Xue, and W. Che, "An 11–40-GHz high-power switch with miniaturized high-order topology using 100-nm GaN-on-Si HEMTs," *IEEE Trans. Electron Devices*, vol. 69, no. 11, pp. 6217–6224, Nov. 2022, doi: 10.1109/TED.2022.3204511.

[22] K.-Y. Lin, W.-H. Tu, P.-Y. Chen, H.-Y. Chang, H. Wang, and R.-B. Wu, "Millimeter-wave MMIC passive HEMT switches using traveling-wave concept," *IEEE Trans. Microw. Theory Techn.*, vol. 52, no. 8, pp. 1798–1808, Aug. 2004, doi: 10.1109/tmtt.2004.831574.

[23] M. J. Schindler and A. Morris, "DC-40 GHz and 20–40 GHz MMIC SPDT switches," *IEEE Trans. Microw. Theory Techn.*, vol. MTT-35, no. 12, pp. 1486–1493, Dec. 1987, doi: 10.1109/tmtt.1987.1133879.

[24] Y. Wang, P. Tripathi, H.-W. Lei, and H. Wang, "Broadband SPST switches in 250-nm GaN HEMT process," in *Proc. Asia–Pacific Microw. Conf. (APMC)*, Nov. 2022, pp. 680–682, doi: 10.23919/APMC55665.2022.9999952.

[25] A. S. A. Fletcher and D. Nirmal, "A survey of gallium nitride HEMT for RF and high power applications," *Superlattices Microstructures*, vol. 109, pp. 519–537, Sep. 2017, doi: 10.1016/j.spmi.2017.05.042.

[26] G. Cywiński, K. Szkudlarek, P. Kruszewski, I. Yahniuk, S. Yatsunenko, G. Muzioł, C. Skierbiszewski, W. Knap, and S. L. Rumyantsev, "Low frequency noise in two-dimensional lateral GaN/AlGaN Schottky diodes," *Appl. Phys. Lett.*, vol. 109, no. 3, Jul. 2016, Art. no. 033502, doi: 10.1063/1.4958857.

[27] Y. Yashchyshyn, P. Bajurko, J. Sobolewski, P. Sai, S. Rumyantsev, and G. Cywinski, "AlGaN/GaN Schottky barrier single-pole single-throw RF switch," in *Proc. 24th Int. Microw. Radar Conf. (MIKON)*, Sep. 2022, pp. 1–3, doi: 10.23919/MIKON54314.2022.9925012.

[28] D. M. Pozar, *Microwave Engineering*, 4th ed. New York, NY, USA: Wiley, 2012.
[29] G. Shen, W. Che, H. Zhu, F. Xu, and Q. Xue, "Analytical design of millimeter-wave 100-nm GaN-on-Si MMIC switches using FET-based resonators and coupling matrix method," *IEEE Trans. Microw. Theory Techn.*, vol. 69, no. 7, pp. 3307–3318, Jul. 2021, doi: 10.1109/TMTT.2021.3081113.
[30] G. Shen, H. Ma, X. Wang, F. Xu, and H. Zhu, "Wideband millimeter-wave SPST switch in 100-nm GaN-on-Si using strong mutual coupling," *IEEE Trans. Circuits Syst. II, Exp. Briefs*, vol. 70, no. 6, pp. 1891–1895, Jun. 2023.
[31] A. Margomenos, A. Kurdoghlian, M. Micovic, K. Shinohara, H. Moyer, D. C. Regan, R. M. Grabar, C. McGuire, M. D. Wetzel, and D. H. Chow, "W-band GaN receiver components utilizing highly scaled, next generation GaN device technology," in *Proc. IEEE Compound Semiconductor Integr. Circuit Symp. (CSICS)*, Oct. 2014, pp. 1–4, doi: 10.1109/CSICS.2014.6978585.
[32] T. Sonnenberg, A. Romano, S. Verploegh, M. Pinto, and Z. Popovic, "*V*- and *W*-band millimeter-wave GaN MMICs," *IEEE J. Microw.*, vol. 3, no. 1, pp. 453–465, Jan. 2023, doi: 10.1109/jmw.2022.3221281.

PAWEŁ BAJURKO (Member, IEEE) received the M.Sc. and Ph.D. degrees in telecommunication from the Warsaw University of Technology (WUT), Warsaw, Poland, in 2004 and 2012, respectively.

Since 2012, he has been an Assistant Professor with the Institute of Radioelectronics and Multimedia Technology, WUT. In 2022, he joined the Institute of High Pressure Physics of the Polish Academy of Sciences. His research interests include antenna techniques, the design and measurement examination of GaN-based devices, terahertz detection, microwave and millimeter wave measurement techniques, and wireless localization.

JAKUB SOBOLEWSKI (Member, IEEE) received the B.S. degree in electronics engineering from the Bialystok University of Technology, Bialystok, Poland, in 2014, and the M.S. and Ph.D. degrees in telecommunications from the Warsaw University of Technology (WUT), Warsaw, Poland, in 2017 and 2022, respectively.

In 2022, he joined the Institute of High Pressure Physics of the Polish Academy of Sciences, and the Institute of Radioelectronics and Multimedia Technology, WUT, in 2023. His research interests include the microwave and millimeter wave antenna design, microwave material characterization, millimeter wave integrated circuits, and integration of high frequency devices.

YEVHEN YASHCHYSHYN (Senior Member, IEEE) received the M.E. degree from Lviv Polytechnic National University, Lviv, Ukraine, in 1979, the Ph.D. degree from the Moscow Institute of Electronics and Mathematics, Moscow, Russia, in 1986, and the D.Sc. (Habilitation) degree from the Warsaw University of Technology (WUT), Warsaw, Poland, in 2006.

Since 1999, he has been with the Institute of Radioelectronics and Multimedia technology, WUT, where he is currently a Professor and the Head of the Sub-Terahertz Technology Division. He has authored more than 250 technical articles and has authored or coauthored five books. He holds several patents. His current research interests include antenna theory and techniques, smart beamforming, reconfigurable antennas, radio-over-fiber techniques, and materials characterization, including ferroelectric ceramic-polymers composites investigation up to sub-terahertz frequency.

PAVLO SAI received the master's degree in physics from the Faculty of Physics and Mathematics, Zhytomyr Ivan Franko State University, in 2015. He is currently pursuing the Ph.D. degree with the THz Laboratory, Institute of High Pressure Physics of the Polish Academy of Sciences.

He has three years' experience as an Engineer with the Laboratory of Physical and Technological Problems of Solid-State Microwave Electronics, V. E. Lashkaryov Institute of Semiconductor Physics, NAS, Ukraine. In 2018, he joined the CENTERA Project, as an Assistant. His main scientific interests include GaN-based plasmonic devices for terahertz spectral range application, grating metamaterials for amplification and generation of terahertz radiation, AlGaN/GaN high electron mobility transistors with graphene integration, and ohmic and barrier contact to III-Nitride group of semiconductor materials.

SERGEY L. RUMYANTSEV received the M.S.E.E. degree from the Leningrad Electrotechnical Institute, Petersburg, in 1977, the Ph.D. degree in physics and in mathematics from the Leningrad Polytechnical Institute, in 1986, and the D.Sc. (Habilitation) degree in electronics from the A. F. Ioffe Institute of Physics and Technology, Leningrad, in 1996.

From 1977 to 1980, he was with the A. F. Ioffe Physico-Technical Institute. From 1977 to 1989, he was with Industrial and Scientific Corporation "Svetlana." From 1989 to 2018, he was a Research Fellow with the A. F. Ioffe Physico-Technical Institute. From 1999 to 2018, he was a Professor with the Rensselaer Polytechnic Institute, USA. Since 2018, he has been a Professor with the Institute of High Pressure Physics of the Polish Academy of Sciences.

TEODOR NARYTNYK received the degree in semiconductors and dielectrics from the Faculty of Radioelectronics, Kyiv University of Technology, the master's degree from the Faculty of Radiophysics, Taras Shevchenko Kyiv National University, and the Ph.D. degree in technical sciences. He defended his master's thesis with a special Scientific Council of the Research Institute "Istok" (Russian Federation), in 1979.

His research was devoted to paraelectric active elements for use in radio-electronic devices and special-purpose systems. The work is focused on the study of radio-electronic devices and systems, dielectronic and microelectronics, microwave technology, and terahertz telecommunication technologies.

GRZEGORZ CYWIŃSKI received the Diploma degree (Hons.) from St. Petersburg, Russia, in 1995, the bachelor's and M.Sc. (Eng.) degrees in microelectronics and semiconductor instruments, and the Ph.D. degree in semiconductor physics from the Institute of Physics of the Polish Academy of Sciences (PAS), in 2004. He has been a Professor with the Institute of High Pressure Physics PAS, since February 2020. From September 2015 to September 2020, he was an Assistant Professor and the Deputy Head of the Laboratory TeraGaN, Institute of High Pressure Physics PAS. He has 20 years of experience in molecular beam epitaxy (nitrides, tellurides, selenides, and graphene), GaInN/AlInGaN intersubband devices for telecommunication wavelengths, GaN/AlGaN HEMTs for microwave and terahertz ranges, GaN/AlGaN lateral Schottky barrier diodes for frequency multiplication, and mixing GaN/AlGaN FinFET and edgeFET.